Fluorescence Spectroscopy of Epithelial Tissue Throughout the Dysplasia-Carcinoma Sequence in an Animal Model: Spectroscopic Changes Precede Morphologic Changes

Lezlee Coghlan, DVM,[1] Urs Utzinger, PhD,[2] Rebecca Richards-Kortum, PhD,[2]* Carrie Brookner, PhD,[2] Andres Zuluaga, PhD,[2] Irma Gimenez-Conti, DDS, PhD,[3] and Michele Follen, MD, PhD[4]

[1]*Department of Veterinary Sciences, The University of Texas M.D. Anderson Cancer Center, Science Park, Bastrop, Texas*
[2]*Department of Electrical and Computer Engineering and The Biomedical Engineering Program, The University of Texas, Austin, Texas*
[3]*Department of Carcinogenesis, The University of Texas M.D. Anderson Cancer Center, Science Park, Smithville, Texas*
[4]*Department of Gynecologic Oncology, The University of Texas M.D. Anderson Cancer Center, Houston, Texas*

Background and Objective: The hamster cheek pouch carcinogenesis model, using chronic treatments of dimethylbenz[α]anthracene (DMBA) was used as a model system to investigate changes in epithelial tissue autofluorescence throughout the dysplasia-carcinoma sequence.
Study Design/Materials and Methods: Fluorescence emission spectra were measured weekly from 42 DMBA-treated animals and 20 control animals at 337, 380, and 460 nm excitation. A subset of data in which histopathology was available was used to develop diagnostic algorithms to separate neoplastic and non-neoplastic tissue. The change in fluorescence intensity over time was examined in all samples at excitation-emission wavelength pairs identified as diagnostically useful.
Results: Algorithms based on autofluorescence can separate neoplastic and non-neoplastic tissue with 95% sensitivity and 93% specificity. Greatest contributions to diagnostic algorithms are obtained at 380 nm excitation, and 430, 470, and 600 nm emission. Changes in fluorescence intensity are apparent as early as 3 weeks after initial treatment with DMBA, whereas morphologic changes associated with dysplasia occur on average at 7.5–12.5 weeks after initial treatment.
Conclusions: Fluorescence spectroscopy provides a potential tool to identify biochemical changes associated with dysplasia and hyperplasia, which precede morphologic changes observed in histologically stained sections. Lasers Surg. Med. 29:1–10, 2001.

Key words: spectrometry; fluorescence; DMBA; Syrian hamster

INTRODUCTION

Numerous clinical studies have shown that fluorescence spectroscopy shows promise for in vivo detection of epithelial dysplasia [1–3], in organ sites such as the cervix [4,5], the colon [6–8], and the oral cavity [9–12]. In most of these studies, tissue fluorescence is measured before biopsy and then correlated with histologic diagnosis. In many organ sites, interpatient variations in autofluorescence are significant [4,9–10] and make it difficult to identify those spectroscopic features that are most correlated with the development of dysplasia. Because of patient care guidelines, it is not generally permissible to measure fluorescence of a lesion in a single patient as it progresses from normal to abnormal. However, a model of chemically driven carcinogenesis in the Syrian hamster cheek pouch can be used in place of such human studies. This model has the potential to provide a better understanding of how fluorescence spectra change during disease progression, which should provide critical information about when in the dysplasia-carcinoma sequence spectroscopic changes take place.

The hamster cheek pouch carcinogenesis model, using chronic treatments with the carcinogen dimethyl benz [α] anthracene (DMBA) in the cheek pouch, is well characterized [13,14]. Histologically, the 16-week treatment protocol pushes the epithelial lining of the cheek pouch through stages of inflammation, hyperplasia, dysplasia, and both benign and malignant tumor formation. Epithelial hyperplasia develops after only a few treatments with DMBA. Dysplastic lesions, resembling human premalignant lesions, are seen after 6–8 weeks of treatment. After approximately 10 weeks, papillomas and carcinomas begin to appear [13].

Several in vivo studies have been performed in which carcinoma was initiated with DMBA, and then tissue autofluorescence was measured to determine its diagnostic value [15–18]. In early studies [15,16], the cheek pouch tissue was excited with 442 nm light, and fluorescence was collected in the red (>630 nm) and green (520 nm)

Contract grant sponsor: Physician Referral Service Research Support: Contract grant number: 4-0021080; Contract grant sponsor: National Institutes of Health: Contract grant number: CA16672.
*Correspondence to: Rebecca Richards-Kortum, PhD, Department of Electrical and Computer Engineering, The University of Texas at Austin, Austin, TX 78712.
E-mail: kortum@mail.utexas.edu
Accepted 13 September 2000

portions of the spectrum. The ratio of red to green autofluorescence was computed and used to separate tissues into the categories normal, mild dysplasia, moderate dysplasia, severe dysplasia, carcinoma in situ (CIS), and invasive cancer. In one study [15] a sensitivity of 100% and a specificity of 80% were achieved, and in another similar study [16] the sensitivity and specificity were 76% and 83%, respectively. Dhingra et al. [17] measured fluorescence emission spectra in vivo from DMBA-induced precancers and early cancers in the hamster cheek pouch and from human subjects at 410 nm excitation [18]. Neoplastic lesions showed characteristic fluorescence between 630 and 640 nm emission. By using this as a diagnostic criterion, 45 of 49 lesions were correctly diagnosed. These studies showed the potential of autofluorescence in detecting early neoplastic changes in the hamster cheek pouch model.

Our group has shown that fluorescence emission spectra at 337, 380, and 460 nm excitation show promise for in vivo detection of cervical dysplasia, with sensitivity and specificity of 82% and 68% in a series of 95 patients [4]. Although these classification rates are encouraging, they are limited by large interpatient variations in the fluorescence of normal cervical tissue that are not well understood. The goals of this study were to use the hamster cheek pouch model of carcinogenesis to explore changes in autofluorescence at these excitation wavelengths as tissue goes through the dysplasia carcinoma sequence. In this model system, we find that algorithms with high sensitivity and specificity can be developed to differentiate neoplastic and non-neoplastic tissue. Furthermore, changes in fluorescence are apparent as early as 3 weeks after initial DMBA treatment, several weeks earlier than morphologic changes indicative of dysplasia are observed in stained histologic sections.

MATERIALS AND METHODS

Animal Treatment Protocol

This study consisted of 62 Syrian hamsters in two arms; 42 animals were treated with the carcinogen 0.5% DMBA in mineral oil to induce gradual epithelial carcinogenesis, and 20 control animals were treated only with mineral oil. Animals were initially treated three times per week; however, after 2 weeks, treatments were reduced to twice per week, and the concentration of DMBA was reduced to 0.25% because of significant erosion in the DMBA group. In each case, the treatment substance was applied to the right cheek pouch with a no. 5 camel hair brush. On a weekly basis, at least one animal from each arm was killed, and the cheek pouch was surgically removed for histologic analysis (Table 1). This protocol was approved by the Animal Care Use Committee at The University of Texas M.D. Anderson Cancer Center and was conducted at the Department of Veterinary Sciences campus, an Association for the Assessment and Accreditation of Laboratory Animal Care International accredited facility, in accordance with the Guide for the Care and Use of Laboratory Animals.

DMBA Fluorescence

Preliminary experiments were performed to determine whether the fluorescence from DMBA affects in vivo fluorescence measurements of the hamster cheek pouch. A fluorescence excitation-emission matrix was measured from a solution of 0.5% DMBA by using a spectrofluorimeter (SPEX FLUOROLOG II, JY Inc, Edison NJ). Excitation wavelengths ranged from 250 to 500 nm in 10-nm increments, and emission wavelengths ranged from 10 nm past the excitation wavelength to the lower of 10 nm below twice the excitation wavelength or 700 nm, in 5-nm increments. Results showed that DMBA has 4 maxima: two at 270 nm excitation, 410 and 430 nm emission and two at 370 nm excitation, 410 and 430 nm emission. These maxima are distinct from that of untreated cheek pouch tissue. The DMBA was then applied to the cheek pouches of three animals in the same manner to be used in the DMBA arm of the study. Fluorescence emission spectra were measured from the cheek pouches at 24 hours and 48 hours after the application of the DMBA by using the same system used to measure fluorescence from the control and DMBA-treated animals in the full protocol. At 24 hours, residual DMBA fluorescence could be detected in the fluorescence spectra measured from tissue, but at 48 hours no DMBA fluorescence was measured. On the basis of these results, the DMBA treatment days were scheduled to ensure that the fluorescence measurements always took place at least 48 hours after the last treatment.

Hamster Fluorescence Measurements

The fluorescence of the control and DMBA-treated hamster cheek pouches was measured weekly according to the schedule shown in Table 1. Fluorescence emission spectra were measured in vivo at 337, 380, and 460 nm excitation by using a fiber-optic-based fluorimeter. This system, previously described in detail [4], incorporates two pulsed nitrogen pumped dye lasers, an optical fiber probe, and an optical multichannel analyzer (Fig. 1). Each week, fluorescence spectra were measured from a preselected group of animals. The hamster cheek pouch was manually inverted and rinsed with saline solution, the probe was placed in contact with the cheek pouch, and fluorescence spectra were measured.

At the start of each measurement day, a mercury spectrum was measured to permit wavelength calibration of the system. In addition, before measurements from each animal, background spectra and spectra of a Rhodamine standard were collected [4]. All background subtracted spectra were corrected for the nonuniform spectral response of the modified detection system by using correction factors obtained by recording the spectrum of an National Institute of Standards and Technology (N.I.S.T.) traceable calibration tungsten ribbon filament lamp and are reported in arbitrary, calibrated units relative to the peak fluorescence intensity of the Rhodamine standard. After each day of measurements, the probe was disinfected by using Metricide (Metrex Orange, CA). Each day, measure-

TABLE 1. Study Design for the DMBA-Treated and Control Group Animals

Animals DMBA Group	Week 1	2	3	4	5	6	7	8	9	10	11	12	13	14	15	16	17
1	FS (N)																
2	FS (H)																
3	F		FS (U)														
4	F		FS (D)														
5	F		F		FS (D)												
6	F		F		FS (I)												
7	F		F		F		FS (I)										
8	F		F		F		FS (I)										
9	F		F		F		F		FS (II)								
10	F		F		F		F		FS (D)								
11	F		F		F		F		F		FS (CIS)						
12	F		F		F		F		F		FS (CIS)						
13	F		F		F		F		F		F		FS (II)				
14	F		F		F		F		F		F		FS (D)				
15	F		F		F		F		F		FS (I)						
16	F		F		F		F		F		F		F		FS (D)		
17	F		F		F		F		F		F		F		F		FS (CIS)
18	F		F		F		F		F		F		F		F		FS (SCC)
19	F		F		F		F		F		F		F		F		FS (SCC)
20	F		F		F		F		F		F		F		F		FS (SCC)
21	F		F		F		F		F		F		F		F		FS (SCC)
22		FS (U)															
23		FS (INF)															
24		F		FS (D)													
25		F		FS (D)													
26		F		F		FS (II)											
27		F		F		FS (II)											
28		F		F		F		FS (II)									
29		F		F		F		F		FB (II)	F	F	F	F	F	F	FS (SCC)
30		F		F		F		F		FS (II)							
31		F		F		F		F		FS (III)							
32		F		F		F		F		F		FS(III)					
33		F		F		F		F		F		FS (III)					
34		F		F		F		F		F		F		FS (II)			
35		F		F		F		F		F		F		FS (CIS)			
36		F		F		F		F		F		F		FS (III)			
37		F		F		F		F		FB (III)	F	F	F	F	F	FS (SCC)	
38		F		F		F		F		FB (II)	F	F	F	F	F	F	FS (SCC)

TABLE 1. (*Continued*)

Animals DMBA Group	Week 1	2	3	4	5	6	7	8	9	10	11	12	13	14	15	16	17
39		F		F		F		F		FS (D)							
40		F		F		F		FB (CIS)	F	F	FS (III)						
41		F		F		F		FB (III)	F	F	F	F	F	FS (CIS)			
42		F		F		F		FB (II)	FS (III)								
Animal Control Group																	
43	F		FS (N)														
44	F		F		FS (N)												
45	F		F		F		FS (N)										
46	F		F		F		F		FS (N)								
47	F		F		F		F		F		F		F		F		FS (INF)
48	F		F		F		F		F		F		FS (INF)				
49	F		F		F		F		F		F		F		FS (N)		
50	F		F		F		F		F		F		F		F		FS (N)
51	F		F		F		F		F		FS (H)						
52	F		F		F		F		F		F		F		F		FS (N)
53		F		FS (N)													
54		FS (N)															
55		F		F		F		FS (N)									
56		F		F		F		F		FS (H)							
57		F		F		F		F		FB (N)	F	F	FS (INF)				
58		F		F		F		F		FB (H)	F	F	F	F	F	FS (N)	
59		F		F		F		F		FB (H)	F	F	F	F	F	F	FS (N)
60		F		F		F		FB (N)	F	F	FS (INF)						
61		F		F		F		FB (N)	F	F	F	F	F	FS (N)			
62		F		F		F		FB (N)	F	F	F	F	F	F	F	F	FS (N)

F = fluorescence measurement, FS = fluorescence measurement and sacrifice, FB = fluorescence measurement and biopsy. Histopathologic diagnoses are shown in parentheses, where N = normal, INF = inflammation, U = ulceration, H = hyperplasia, I = grade I dysplasia, II = grade II dysplasia, III = grade III dysplasia, CIS = carcinoma in situ, and SCC = squamous cell carcinoma. Discrepant diagnoses are indicated with D. Shaded boxes indicate those measurements used in algorithm development.

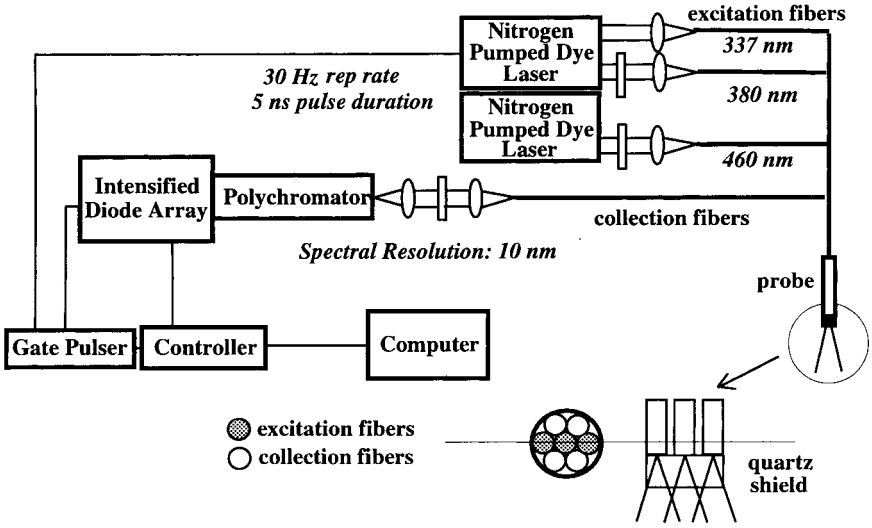

Fig. 1. Schematic diagram of the fiber-optic spectroscopy system used to measure hamster spectra in vivo.

ments were made from the control group first, to prevent transmission of residual DMBA to these animals.

Histological Evaluation

Excised hamster cheek pouches and biopsy samples were fixed with formalin, sectioned, and stained with hematoxylin and eosin for histologic evaluation. Slide reviewers (I.G.C. and L.G.C.) were blinded to the spectroscopic results. Samples were classified into nine categories based on the most severe histopathologic finding: normal, inflammation, ulceration, hyperplasia, dysplasia (grades I–III), CIS, and squamous cell carcinoma (SCC). Discrepant diagnoses between the slide reviewers were noted, and fluorescence measurements from these sites were not used for algorithm development.

Data Analysis

The spectroscopic data were used to develop a diagnostic algorithm to classify samples as either neoplastic or non-neoplastic. Data were included in the algorithm development if corresponding pathology was available and if both histopathologic diagnoses agreed that the sample was either neoplastic or not. Because fluorescence from an animal may have been measured up to nine times before it was biopsied or killed, histopathology was not available for each date that fluorescence was measured. For the purpose of the algorithm development and evaluation, the data were classified into one of two classes: non-neoplastic (normal, inflammation, ulceration, hyperplasia) and neoplastic (all grades of dysplasia, CIS, and SCC). If histopathology indicated a site was non-neoplastic, then all measurements preceding that date were assumed to be non-neoplastic. If histopathology indicated a site was neoplastic, then all measurements after that date were assumed to have neoplasia.

The diagnostic algorithm was developed after the methodology previously developed by Ramanujam et al. [4] to classify spectral data measured from the human cervix. The first step in the algorithm development is data preprocessing. Here, five different normalization methods were used to determine which would result in an algorithm with the best performance. These normalization methods were as follows: (1) normalize each emission spectrum by its peak emission intensity,[1] (2) normalize each emission spectrum to the overall peak intensity of the three emission spectra taken together, (3) normalize each emission spectrum to the peak intensity of the emission spectrum at 337 nm excitation, (4) normalize each emission spectra to the peak intensity of the emission spectrum at 380 nm excitation, and (5) normalize each emission spectrum to the peak intensity of the emission spectrum at 460 nm excitation. Algorithms were also developed with unnormalized data, reported in calibrated units relative to the Rhodamine standard.

After preprocessing, diagnostic algorithms were developed in the following way. A data matrix was created where each row corresponded to the preprocessed fluorescence spectra of each sample, concatenated into a single vector [19]. The associated covariance matrix was calculated and decomposed into eigenvalues and eigenvectors accounting for 99% of the variance in the data. The data matrix was then multiplied by the eigenvector matrix, yielding a set of principal component (PC) scores for each sample. A classification algorithm based on the PC scores was developed. The classification was based on the Maha-

[1]Sometimes significant porphyrin fluorescence was observed near 630 nm emission; this spectral region was excluded when identifying the maximum fluorescence intensity for normalization purposes, because it was not consistently observed.

lanobis distance, which is a multivariate measure of the separation of a point from the mean of a data set in n-dimensional space [20]. The sample was classified to the group from which it was the shorter Mahalanobis distance. To select which PC scores to use in the algorithm, the single PC score giving the best initial performance was identified from the pool of available scores. Each additional PC was then added sequentially, and the one that most improved the diagnostic performance was identified. This process was repeated until performance was no longer improved by the inclusion of additional PC scores or until all available scores were selected. Algorithm performance was quantified by taking the sum of the sensitivity and specificity.

The PC scores that proved to be the most diagnostically useful were then further examined. The component loadings of these PCs were calculated and plotted to relate the PCs to the original emission spectra. The component loading represents the correlation between the PC and the original preprocessed fluorescence spectra of the data set. Several emission wavelength ranges were identified at each excitation wavelength, which corresponded to regions of strong positive or negative correlation; fluorescence intensities at these wavelengths were plotted for all samples throughout all weeks of the study. The overlap in the distribution of these intensities for the group of non-neoplastic and neoplastic animals was studied by applying a simple threshold classifier and counting the proportion of misclassified samples. This allowed a measure of the ability to separate the two groups through the time course of the treatment.

RESULTS

Histopathology

This study included 42 animals in the DMBA treatment group. A total of 236 measurements were made from this group during the 16-week protocol, and six sites were biopsied in weeks 8–10. From the DMBA group, 64 measurements were included in the algorithm development; 40 of these sites had histology corresponding to the measurement date (1 normal, 1 inflammation, 1 hyperplasia, 2 ulcerations, 4 grade I dysplasias, 10 grade II dysplasias, 8 grade III dysplasias, 6 CIS lesions, and 7 SCCs). Histologically, ulceration, inflammation, and hyperplasia were most commonly seen in DMBA-treated animals killed in weeks 2–5. The average number of treatment weeks required to produce grade I dysplasia was 7.5 ± 2.2 weeks (range 5–11 weeks). This increased to 9.4 ± 2.5 weeks (range 6–13 weeks) for grade II dysplasia, 9.9 ± 2.8 weeks (range 4–14 weeks) for grade III dysplasia, 12.5 ± 2.9 weeks (range 8–17 weeks) for CIS, and 16.9 ± 0.3 weeks (range 16–17 weeks) for SCC.

In the 20 animals of the control group, a total of 135 measurements were made, and 6 animals were biopsied in weeks 8–10. Twenty-six sites of the control group had histology corresponding to the measurement date (18 normal, 4 inflammation, and 4 hyperplasia). Because none of the histological assessments of the tissue biopsies or excised cheek pouches showed dysplastic changes, all 135 measurements from this group were used as normal sites in the algorithm development.

Algorithm Results

Six different algorithms were developed by using six different preprocessing methods. The number of eigenvectors accounting for 99% of the variance in the data ranged from 9 to 21. The principal components included in the algorithm development and the resulting algorithm performance are summarized in Table 2 for each of the six cases. Best performance was achieved by using data normalized to the peak of the emission spectrum at 380 nm excitation (sensitivity = 95%, specificity = 93%). Very similar performance was achieved when the data were normalized to the peak intensity at each excitation wavelength separately (sensitivity = 95%, specificity = 88%). Figure 2 shows average emission spectra of all samples in the control and DMBA-treated groups; here each spectrum has been normalized to the peak intensity of the spectrum obtained at each excitation wavelength (normalization method 1). Normalization of the data changes the variance structure and, therefore, the covariance matrix. In general, normalization increases the effects of subtle changes in the fluorescence line shape; however, it also removes intensity information.

Component Loadings

Component loadings were computed for the important principal components to determine which emission wavelength regions were particularly important. Correlations greater than 0.5 or less than -0.5 were considered significant. Component loadings for PC2 from the data normalized to 380 nm excitation (normalization method 4) are shown in Figure 3. PC2 was positively correlated with emission wavelengths 475–630 nm and 655–670 nm at 380 nm excitation and 490–680 nm emission at 460 nm excitation. PC2 was negatively correlated with emission wavelengths 410–440 nm at 380 nm excitation. Figure 4 shows component loadings were computed for PC1 and PC2 from the data normalized to all excitation wavelengths individually (normalization method 1). Neither PC1 nor PC2 showed significant correlations to any emission wavelengths at 337 and 460 nm excitation. At 380 nm excitation, PC1 showed significant positive correlation from 460 to 600 nm emission, and PC2 showed significant negative correlation from 460 to 510 nm emission.

It is of interest that strong correlations were frequently associated with 380 nm excitation, particularly at emission wavelengths near 430 (Fig. 3), 470 (Fig. 4b), and 600 nm (Fig. 3). Fluorescence intensities at these excitation-emission wavelength combinations were plotted vs. time for all the control and DMBA-treated animals (Fig. 5). From Figure 5a, the intensity at 380 nm excitation, 430 nm emission is higher for the DMBA-treated animals starting at week 3, and the magnitude of the difference tends to increase over the length of the study. There is excellent separation between the two groups at this excitation-emission wavelength combination, and it is surprising that

TABLE 2. Comparison of Algorithm Performance Developed by Using Six Different Normalization Methods

Normalization method	No. of eigenvectors that account for 99% of variance	Eigenvectors used in algorithm	Sensitivity (%)	Specificity (%)	Sum of sensitivity and specificity
(1) Each emission spectrum normalized to its own maximum	21	1, 2	**95**	**88**	**1.83**
(2) Each emission spectrum normalized to maximum of spectrum with greatest fluorescence intensity	15	1, 2, 3 9, 12	96	83	1.79
(3) Each emission spectrum normalized to peak of spectrum of 337 nm excitation	14	2, 3, 9, 13	95	80	1.75
(4) Each emission spectrum normalized to peak of spectrum at 380 nm excitation	10	2, 3, 9, 8, 5	**95**	**93**	**1.88**
(5) Each emission spectrum normalized to peak of spectrum at 460 nm excitation	9	1, 2, 4	100	65	1.65
(6) No normalization	11	1	76	84	1.6

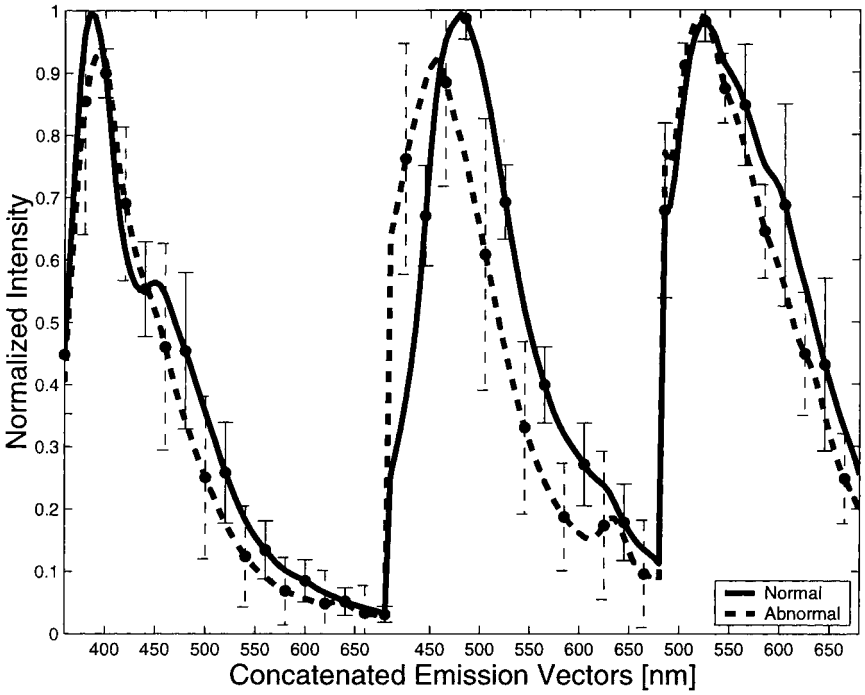

Fig. 2. Average spectra of all sites used to develop the diagnostic algorithm at 337, 380, and 460 nm excitation from left to right; dashed lines represent spectra from the DMBA-treated group, and the solid lines represent spectra from the control group. The error bars represent the standard deviation of the data. Each emission spectrum was normalized to its own maximum (normalization method 1).

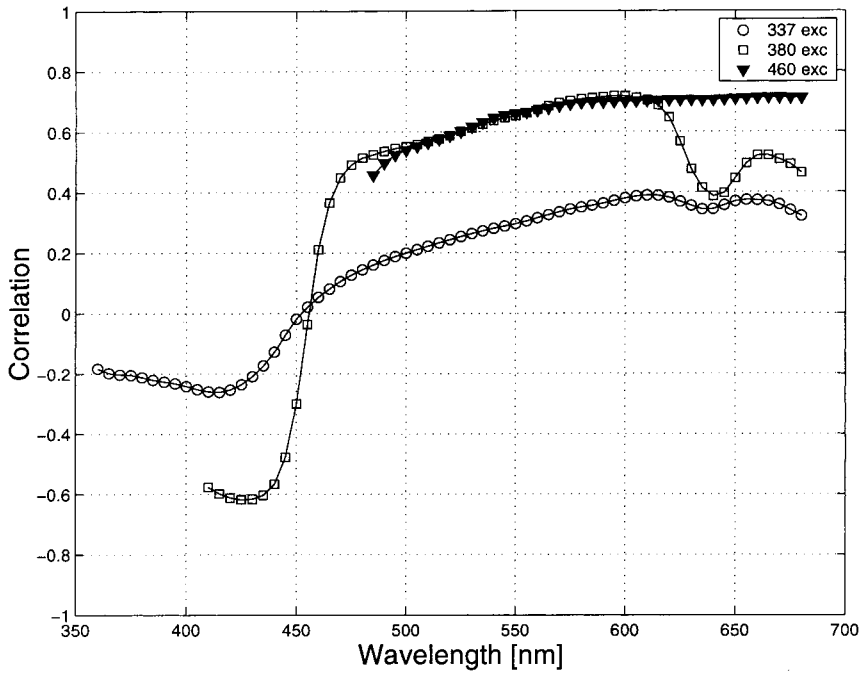

Fig. 3. Component loadings of PC2 for 337 nm excitation, 380 nm excitation, and 460 nm excitation, calculated from the data normalized to 380 nm excitation.

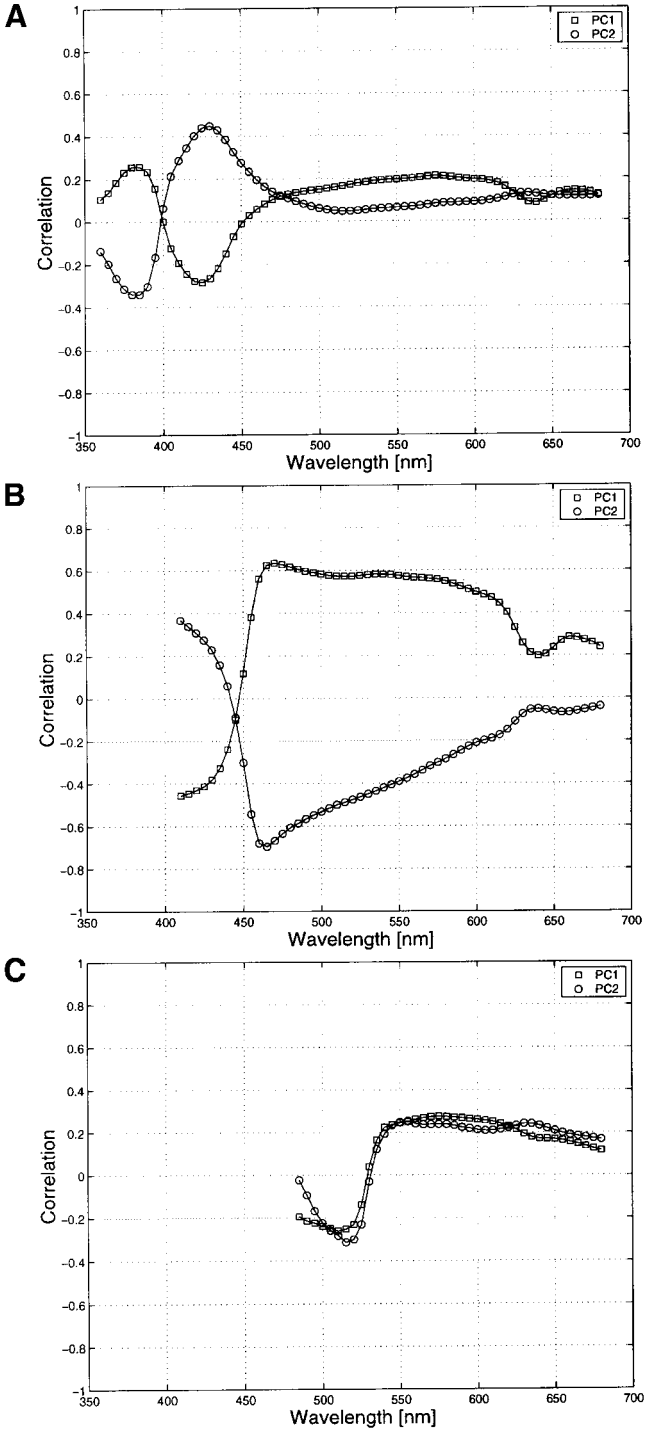

Fig. 4. Component loadings of PC1 and PC2 for (**a**) 337 nm excitation, (**b**) 380 nm excitation, and (**c**) 460 nm excitation, calculated from the data normalized to each excitation wavelength separately.

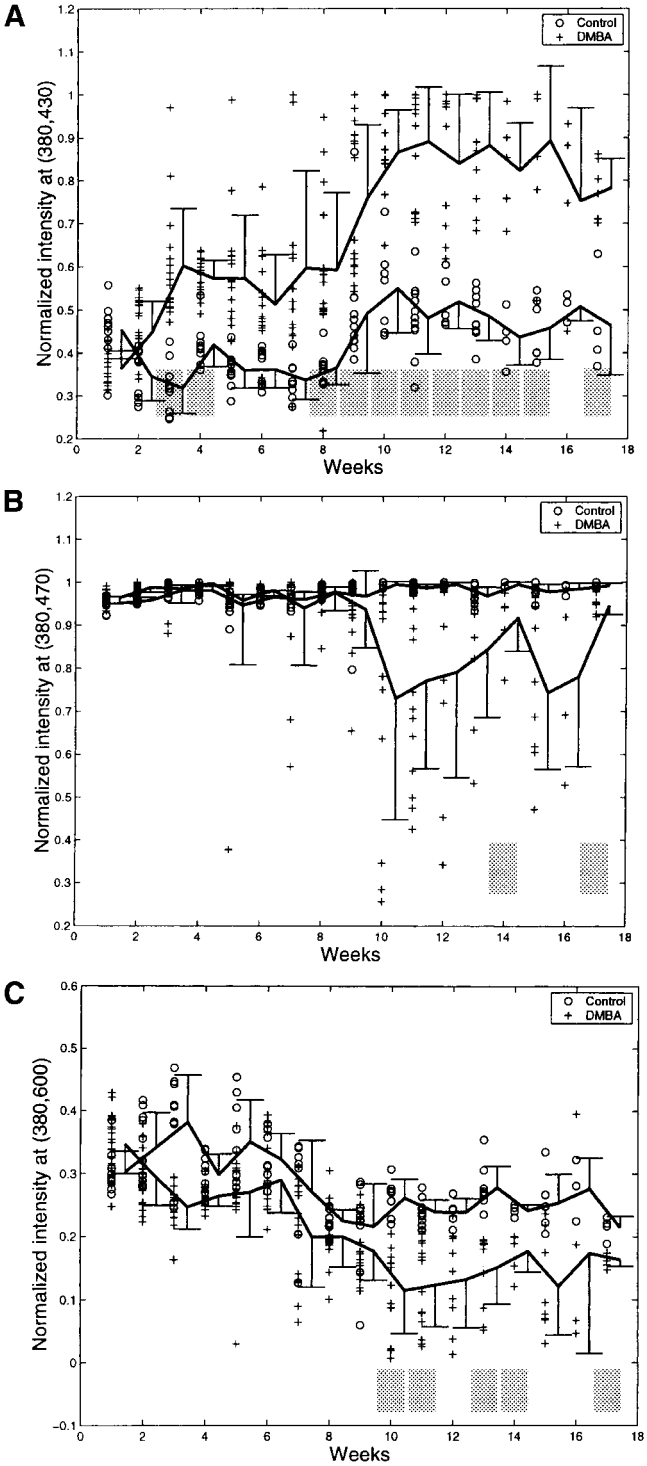

Fig. 5. Fluorescence intensity at 380 nm excitation (**a**) 430 nm emission, (**b**) 470 nm emission, and (**c**) 600 nm emission from all measurements throughout the study. o = control animals and + = DMBA-treated animals. Mean values for each group are connected with a solid line. Standard deviation is indicated in one direction. Gray boxes indicate areas where the control and DMBA data can be separated with less than 7.5% misclassification.

this separation is observed as early as week 3. Weeks where the proportion of samples misclassified is less than 7.5% are marked with gray boxes in Figure 5; in Figure 5a, this separation begins at week 3. In contrast, the intensity at 380 nm excitation, 470 nm emission decreases with time for the DMBA-treated animals, and separation of the mean intensities is seen between the control and DMBA animals beginning in week 9 (Fig. 5b). Similarly, Figure 5c shows a decreased intensity at 380 nm excitation, 600 nm emission in the DMBA-treated animals with separation of the mean intensity from the control animals at weeks 3–5. Beginning at week 10, the proportion of samples misclassified is less than 7.5%.

DISCUSSION AND CONCLUSIONS

This study used an animal model of carcinogenesis to study changes in tissue autofluorescence throughout the dysplasia-carcinoma sequence, information not generally available with human patients. Diagnostic algorithms were developed to determine if the fluorescence measured from neoplastic and non-neoplastic tissue was correlated to the tissue pathology and to determine the most important excitation-emission wavelength combinations. The algorithms performed well, in agreement with previously published studies that show the potential of fluorescence spectroscopy for detecting epithelial dysplastic lesions.

Intensity at 380 nm excitation, 430 nm emission and 380 nm excitation, 600 nm emission were well separated for the two groups as early as week 3. In contrast, the average time for development of grade I dysplasias was 7.5 ± 2.2 weeks. These early differences in fluorescence emission can be based on the development of dysplasia and hyperplastic changes introduced initially by the DMBA treatment. Further studies would be necessary to clearly separate these two effects. Nevertheless, our findings suggest that these excitation-emission pairs may be very useful diagnostically and may be able to detect very early preinvasive neoplastic changes. At 380 nm excitation, 430 nm emission, the DMBA-treated animals showed a higher fluorescence intensity than control animals, whereas at 380 nm excitation, 470 nm emission, the control group showed a more intense fluorescence. This is consistent with a blue-shift in the emission peak of the DMBA-treated animals relative to the peak position for the control animals, and such a shift can be seen in the normalized spectra in Figure 2. Additional studies are needed to definitively assign changes in chromophore concentration responsible for these spectral changes.

ACKNOWLEDGMENTS

The authors thank Donna Schutz, Pam Kille, and Dale Weiss for assistance with in vivo procedures, Jimi Lynn Rosborough-Brandon for histological services, and Holger Fuchs for assistance in acquiring data.

REFERENCES

1. Sevick-Muraca E, Richards-Kortum R. Quantitative optical spectroscopy for tissue diagnosis. Ann Rev Phys Chem 1996; 47:555–606.
2. Wagnieres GA, Star WM, Wilson BC. In vivo fluorescence spectroscopy and imaging for oncological applications. Photochem Photobiol 1998;68:603–632.
3. Stepp H, Sroka R, Baumgartner R. Fluorescence endoscopy of gastrointestinal diseases: basic principles, techniques, and clinical experience. Endoscopy 1998;30:379–386.
4. Ramanujam N, Follen-Mitchell M, Mahadevan-Jansen A, Thomsen S, Staerkel G, Malpica A, Wright T, Atkinson N, Richards-Kortum R. Cervical precancer detection using multivariate statistical algorithm based on laser-induced fluorescence spectra at multiple excitation wavelengths. Photochem Photobiol 1996;64:720–735.
5. Agrawal A, Utzinger U, Brookner C, Pitris C, Mitchell MF, Richards-Kortum R. Fluorescence spectroscopy of the cervix: influence of acetic acid, cervical mucus, and vaginal medications. Lasers Surg Med 1999;25:237–249.
6. Schomacker K, Frisoli J, Compton C, Flotte T, Richter J, Nishioka N, Deutsch T. Ultraviolet laser-induced fluorescence of colonic tissue: basic biology and diagnostic potential. Lasers Surg Med 1992;12:63–78.
7. Wang TD, Crawford JM, Feld MS, Wang Y, Itzkan I, Van Dam J. In vivo identification of colonic dysplasia using fluorescence endoscopic imaging. Gastrointest Endosc 1999;49: 447–455.
8. Mycek MA, Schomacker KT, Nishioka NS. Colonic polyp differentiation using time-resolved autofluorescence spectroscopy. Gastrointest Endosc 1998;48:390–394.
9. Schantz SP, Kolli V, Savage HE, Yu G, Shah JP, Harris DE, Katz A, Alfano RR, Huvos AG. In vivo native cellular fluorescence and histological characteristics of head and neck cancer. Clin Cancer Res 1998;4:1177–1182.
10. Gillenwater A, Jacob R, Ganeshappa R, Kemp B, El-Naggar AK, Palmer JL, Clayman G, Mitchell MF, Richards-Kortum R. Noninvasive diagnosis of oral neoplasia based on fluorescence spectroscopy and native tissue autofluorescence. Arch Otolaryngol Head Neck Surg 1998;124:1251–1258.
11. Kolli V, Savage HE, Yao TJ, Schantz SP. Native cellular fluorescence of neoplastic upper aerodigestive mucosa. Arch Otolaryngol Head Neck Surg 1995;121:1287–1292.
12. Ingrams DR, Dhingra JK, Roy K, Perrault DF Jr, Bottrill ID, Kabani S, Rebeiz EE, Pankratov MM, Shapshay SM, Manoharan R, Itzkan I, Feld MS. Autofluorescence characteristics of oral mucosa. Head Neck 1997;19:27–32.
13. Zenklusen JC, Stockman SL, Fischer SM, Conti CJ, Gimenez-Conti IB. Transforming growth factor-beta 1 expression in Syrian hamster cheek pouch carcinogenesis. Mol Carcinog 1994;9:10–16.
14. Gimenez-Conti IB, Shin DM, Bianchi AB, Roop DR, Hong WK, Conti CJ, Slaga TJ. Changes in keratin expression during 7,12-dimethylbenz[a]anthracene-induced hamster cheek pouch carcinogenesis. Cancer Res 1990;50:4441–4445.
15. Kluftinger AM, Davis NL, Quenville NF, Lam S, Hung J, Palcic B. Detection of squamous cell cancer and precancerous lesions by imaging of tissue autofluorescence in the hamster cheek pouch model. Surg Oncol 1992;1:183–188.
16. Pathak I, Davis NL, Hsiang YN, Quenville NF, Palcic B. Detection of squamous neoplasia by fluorescence imaging comparing porfimer sodium fluorescence to tissue autofluorescence in the hamster cheek-pouch model. Am J Surg 1995;170:423–426.
17. Dhingra JK, Zahng X, McMillan K, Kabani S, Manoharan R, Itzkan I, Feld MS, Sharpshay SM. Diagnosis of head and neck precancerous lesions in an animal model using fluorescence spectroscopy. Laryngoscope 1998;108:471–475.
18. Dhingra JK, Perrault DF, McMillan K, Rebeiz EE, Kabani S, Manoharan R, Itzkan I, Feld MS, Shapshay SM. Early diagnosis of upper aerodigestive tract cancer by autofluorescence. Arch Otolaryngol Head Neck Surg 1996;122:1181–1186.
19. Ramanujam N, Follen Mitchell M, Mahadevan A, Thomsen S, Malpica A, Wright T, Atkinson N, Richards-Kortum R: Development of a multivariate statistical algorithm to analyze human cervical tissue fluorescence spectra acquired in vivo. Lasers Surg Med 1996;19:46–62.
20. Dillon RW, Goldstein M. Multivariate Analysis: Methods and Applications. New York: John Wiley and Sons; 1984.